



Article

Effects of Infill Density and Pattern on the Tensile Mechanical Behavior of 3D-Printed Glycolyzed Polyethylene Terephthalate Reinforced with Carbon-Fiber Composites by the FDM Process

Mohamed Daly ^{1,2}, Mostapha Tarfaoui ^{1,3,*}, Mountasar Bouali ⁴ and Amine Bendarma ^{5,6}

¹ National School of Advanced Techniques Brittany, IRDL, UMR CNRS 6027, F-29200 Brest, France; mohamed.daly@ensta-bretagne.org

² Mechanics Laboratory of Sousse, National School of Engineering of Sousse, University of Sousse, Sousse 4023, Tunisia

³ Green Energy Park (IRESEN/UM6P), km2 R206, Benguerir 43150, Morocco

⁴ Aviation School of Borj el Amri, Bab Mnara, La Kasba, Tunis 1008, Tunisia; mos.bendahi@gmail.com

⁵ Laboratory for Sustainable Innovation and Applied Research, Universiapolis, Technical University of Agadir, Bab Al Madina, Qr Tilila, BP 8143, Agadir 80000, Morocco; b.amine@e-polytechnique.ma

⁶ Institute of Structural Analysis, Poznan University of Technology, Piotrowo 5, 60-965 Poznan, Poland

* Correspondence: mostapha.tarfaoui@ensta-bretagne.fr

Abstract: The impacts of infill patterns and densities on the mechanical characteristics of items created by material extrusion additive manufacturing systems were investigated in this study. It is crucial to comprehend how these variables impact a printed object's mechanical characteristics. This work examined two infill patterns and four densities of 3D-printed polyethylene terephthalate reinforced with carbon-fiber specimens for their tensile characteristics. Rectilinear and honeycomb infill designs were compared at 100%, while each had the following three infill densities: 20%, 50%, and 75%. As predicted, the findings revealed that as the infill densities increased, all analyzed infill patterns' tensile strengths and Young's moduli also increased. The design with a 75% honeycomb and 100% infill density has the highest Young's modulus and tensile strength. The honeycomb was the ideal infill pattern, with 75% and 100% densities, providing significant strength and stiffness.

Keywords: additive manufacturing; CF/PETG; infill pattern effect; infill density effect



Citation: Daly, M.; Tarfaoui, M.; Bouali, M.; Bendarma, A. Effects of Infill Density and Pattern on the Tensile Mechanical Behavior of 3D-Printed Glycolyzed Polyethylene Terephthalate Reinforced with Carbon-Fiber Composites by the FDM Process. *J. Compos. Sci.* **2024**, *8*, 115. <https://doi.org/10.3390/jcs8040115>

Academic Editor: Yuan Chen

Received: 8 February 2024

Revised: 8 March 2024

Accepted: 18 March 2024

Published: 22 March 2024



Copyright: © 2024 by the authors. Licensee MDPI, Basel, Switzerland. This article is an open access article distributed under the terms and conditions of the Creative Commons Attribution (CC BY) license (<https://creativecommons.org/licenses/by/4.0/>).

1. Introduction

To improve the manufacturing process for all human endeavors, new technologies and solutions must be developed for civilization to advance. Traditionally, honeycombs or other composite materials are produced via extrusion, welding, or injection molding [1]. In this regard, additive manufacturing (AM) is a revolutionary technological advancement that is revolutionizing the production of goods. Mass customization, complex designs and geometries, waste reduction, supply chain simplification, quicker time to market, drastic assembly reduction, weight reduction (topology optimization), and low-volume manufacturing are just a few advantages of additive manufacturing (AM) over traditional manufacturing processes that are driving the revolution [2,3].

AM technology is now widely used in academic research as well as in several engineering applications, including the mechanical [4], biomedical [5–8], construction [9], aerospace, and food sectors [10]. Moreover, recycling and reusing thermoplastic composite materials at both high and low temperatures is known as additive manufacturing [11–13].

Binder jetting, direct energy deposition, material extrusion, material jetting, powder bed fusion, sheet lamination, and vat photopolymerization are the seven basic processing techniques used in AM based on printing technology [14].

Fused deposition modeling (FDM) is an extrusion-based technique for creating polymer-based models and structures [15]. The model that will be produced is transformed into a design model for the FDM printing technique and imported into the slicing program [16].

Several factors must be considered, including build orientation, nozzle diameter, printing speed, layer thickness, and extrusion temperature. The primary material used in FDM technology is a filament which is turned into a semi-liquid condition and injected into a nozzle that travels by the commands of the slicing program.

The material extruded from the nozzle is deposited layer-by-layer to print the entire model. Figure 1 depicts a schematic representation of the FDM process [17].

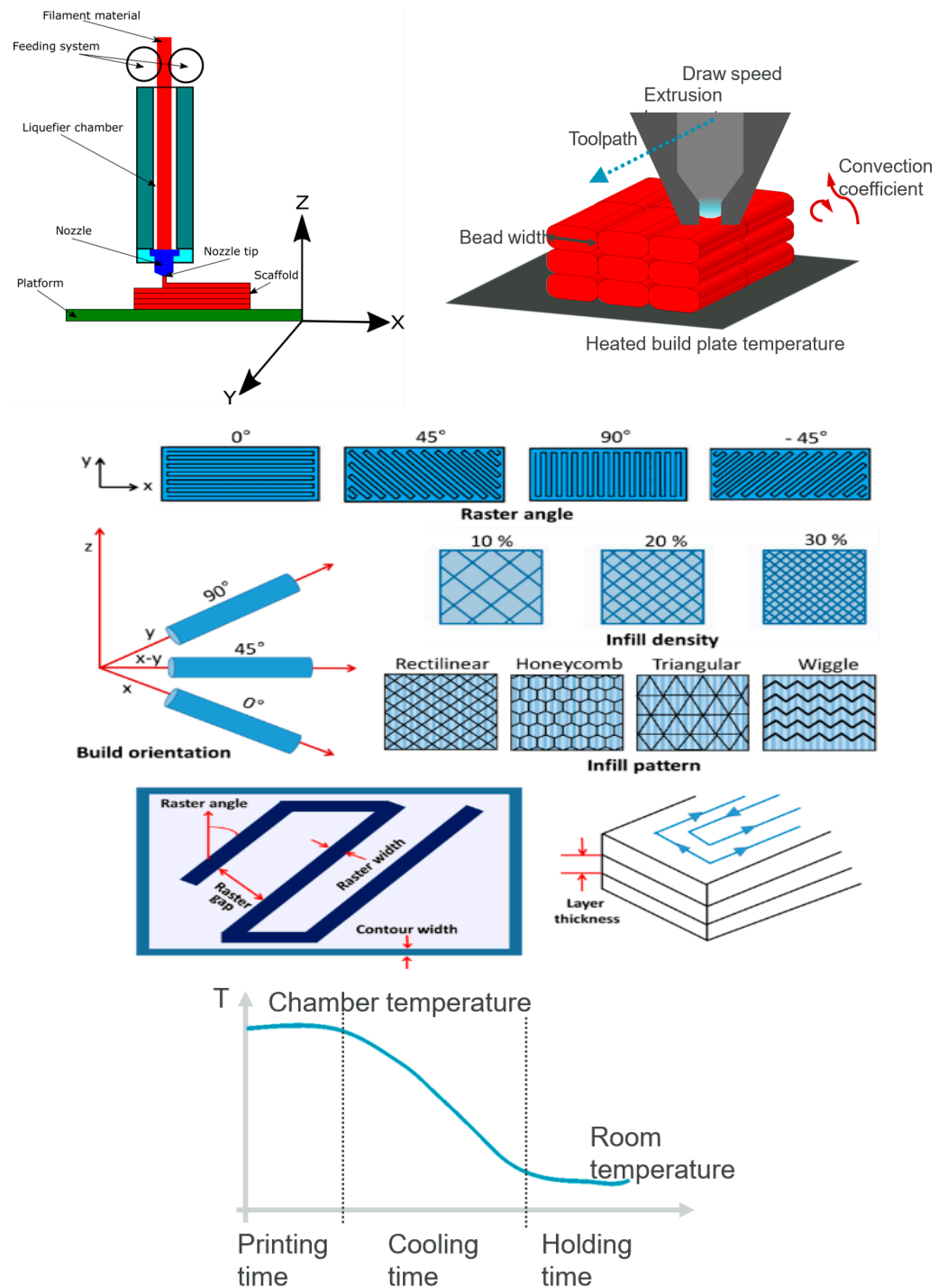


Figure 1. Schematic representation of the FDM process and its parameters.

When considering infill, one must consider the unique relationship between strength, cost, and print time. Every increase in an object's strength increases the printing cost and time. The key to successful infill use is finding a balance where sufficient strength is procured for an object's intended purpose while keeping the cost and time within reasonable bounds.

One of the most popular infill patterns is the 3D honeycomb infill. It is regarded as the most widely used and potent infill pattern. This standard infill pattern offers sufficient rigidity in all directions. It is also one of the most straightforward infill patterns to print, requiring only a tiny amount of bridging from a print head.

Several academic works have studied the static and dynamic behaviors of honeycombs made via additive manufacturing. The impacts of infill density and print orientation on the mechanical behavior of finished items have been the subject of several research works [18,19].

A filling density is the percentage by which a container's interior will be filled. Its primary influence is the overall resistance of the piece. However, the filling rate will be factored into the calculation of the print duration, as well as the final cost of the piece. The greater the density, the greater the amount of filament required. The filling density will also affect the weight of a piece.

A frequently asked question whether or not the importance of the filling density is related to the final resistance of a piece, and if so, why not use a 100% filling density for all impressions. In simple terms, the time it takes to print and the cost of consumables make using a 3D printer unprofitable. Furthermore, a 100% filling may cause a slight deformation in the printed piece, resulting in a change in the exterior linearity of the surface.

Furthermore, it is not only the filling density that influences the behavior of a 3D-printed sample. The evolution of the filling density is not always proportional to the evolution of the resistance, depending on the shape of the piece. Even if the filling density significantly impacts the final resistance, a filling density greater than 80% is not always recommended. According to 3DHubs, the resistance of a piece with a 50% filling rate increases by 25% compared to a piece with a 25% filling density. However, between a filling density of 50% and a filling density of 75%, the resistance increases by only 10%.

There are numerous geometries and shapes available for filling out samples. These themes each have their advantages and are intended for specific applications. The critical thing to remember when selecting a filling motif is to consider the use that will be made of the impression. Furthermore, the motif must be associated with a high fill rate to obtain satisfactory results.

Khan et al. [20] found that the honeycomb (also known as hexagonal) infill pattern for printed acrylonitrile butadiene styrene (ABS) specimens had the lowest tensile strength compared to rectilinear and concentric patterns. This could have been because more voids were printed with this infill pattern inside the specimen. Rismalia et al. [21] demonstrated that increasing infill densities improved the three infill patterns' tensile properties. Tensile properties are affected by infill patterns. Compared to the other two patterns, the concentrate infill pattern has the highest tensile properties, while the grid and tri-hexagonal patterns have similar levels.

Yang et al. [22] investigated the mechanical characteristics of additively manufactured 3D re-entrant honeycomb auxetic structures. By using additive manufacturing (AM), Fadida et al. [23] examined the mechanical aspects of samples of Ti6Al4V under static and dynamic compression. The findings demonstrated that when exposed to dynamic and static loads, the dense material created by a laser had superior resistance to the identical traditional material, but their ductility was equivalent.

The impact strength of PLA specimens created by additive manufacturing at various printing rates was investigated by Tsouknidas et al. [24]. The PLA sample was subjected to a compressive load. The investigation showed that printing at the slowest pace produced the highest compressive strength.

Using desktop 3D printing, Fernandez et al. [25] examined the impact of infill density on the tensile mechanical response. To determine how nonlinear scaling affected the stiffness of soft cellular structures, Wyatt et al. [26] conducted a study. The results showed a high correlation between the experimental findings and the finite element simulation.

A honeycomb structure constructed from polycaprolactone using additive manufacturing was shown by Zhang et al. [27] to recover up to 80% of its volume following a single compression to densification.

To evaluate the ability of the honeycomb structure Ti6Al4V produced by laser-engineered net shaping (LENSTM) to absorb impact energy, Dudka et al. [28] recently examined the static and dynamic behaviors of the structure. To completely comprehend the compressive behavior of 3D-printed thermoplastic polyurethane honeycombs with different densities, Simon and colleagues [29] conducted experimental research. The outcomes showed that the TPU constructions with different densities could offer adequate impact protection in challenging environmental circumstances.

A study by Yu et al. [30] showed that the analyzed additively manufactured gyroid samples had high dynamic compression-energy absorption capacities. In contrast, the analyzed gyroid structure's energy absorption was on par with that of a uniform gyroid structure.

To replace structures made with standard techniques with 3D-printed structures, it is fundamental to identify the optimal parameters for 3D printing; that is, printed structures must have properties that are equivalent to traditional structures. Many scientific and technical challenges must be met to achieve this goal, and they must go through the phases of characterization of these materials and quantify their performance. A detailed study of the bibliographical references showed no significant works on the mechanical behavior of honeycomb and rectilinear composites produced by 3D printing under quasi-static loads.

Using the INSTRON machine, a series of uniaxial tensile tests were carried out on polyethylene terephthalate reinforced with carbon-fiber (CF/PETG) composite specimens produced by the FDM technique in 3D printing. From the perspective of developing a new generation of lightweight materials with optimal mechanical performances, two parameters were studied in this paper: (1) the effect of the geometry (Nida vs. rectilinear) and (2) the filling density (20%, 50%, 75%, and 100%). This paper aimed to characterize the mechanical and fracture behaviors of the different types of specimens, particularly their Young's moduli, stiffness, maximum loads, and displacements at the breaks. A comparison between Nida and rectilinear fillers and an evaluation of the influence of the percentage of filler on the mechanical behavior of the 3D-printed parts was carried out.

This study intended to show how CF/PETG performs mechanically under tensile loading to strike a compromise between weight, resistance, and mechanical behavior. The material from which a structure is made, its cell shape, its relative density, and several other elements, such as the features of the manufacturing process, the structural boundary, and the loading circumstances, all affect how mechanically strong a structure will be. Similarly, the CF-PETEG product will have reduced tensile strength and yield strength if a designer decides to reduce the filling density from 100% to 75% to save on time and 3D-printed materials. In addition, the results demonstrate that the honeycomb filling pattern has the highest tensile and yield strengths when compared to straight filling. The tensile strengths of the honeycomb and 75% rectilinear fillings were marginally lower than that of the 100% filling.

2. Materials

PETG, also known as glycolic polyester, is a thermoplastic frequently used in additive manufacturing facilities because it combines the ease of PLA printing with the strength of ABS [31]. It is an amorphous plastic with an identical chemical make-up to polyethylene terephthalate, commonly known by its acronym PET, and it can be completely recycled. Glycol was added to lessen its fragility and brittle appearance.

As a result, PETG is a copolymer combining PET and glycol qualities. By including the latter, it is possible to lessen PET’s overheating and, as a result, brittle appearance. PETG’s hardness, chemical and impact resistance, transparency, and ductility make it ideal for 3D printing. It is a thermally stable material that is simple to extrude. In particular, it is valued for being compatible with food contact. Concerning its shortcomings, we note that the PETG requires a heating plate to prevent the warping issues seen with ABS [31].

It is better to utilize a BuildTak sheet to ensure the material hangs, even if the warping rate is modest. In comparison to PLA, it is also more prone to scratches. Also, it keeps well in a cold, dry atmosphere and can quickly absorb moisture. One must be aware that PETG is frequently reinforced with carbon fibers, increasing the part’s rigidity while minimizing the weight of the 3D-printed components.

Our industrial partner provided this option in its selection of filaments. It has also created a carbon-fiber-reinforced PETG that increases rigidity while reducing the matrix’s brittleness [31].

As shown in Table 1, the composite (CF/PETG) was chosen for this study as a material with a high mechanical performance. This substance is regarded as a high-tech engineering polymer.

Table 1. Mechanical properties of the CF/PETG.

Mechanical Properties of the CF/PETG		
Property	Value	Unit
Density	1.08	g/cm ³
Traction modulus	4700	MPa
Bending modulus	3800	MPa
Elongation at break	2	%
Stress at rupture	42	MPa
Poisson’s ratio	0.4	-

3. Structural Design

The specimens displayed in this study were made using the FDM procedure. Figure 2 shows the FDM system operation diagram and the printing system used in our investigation of the printed specimens.

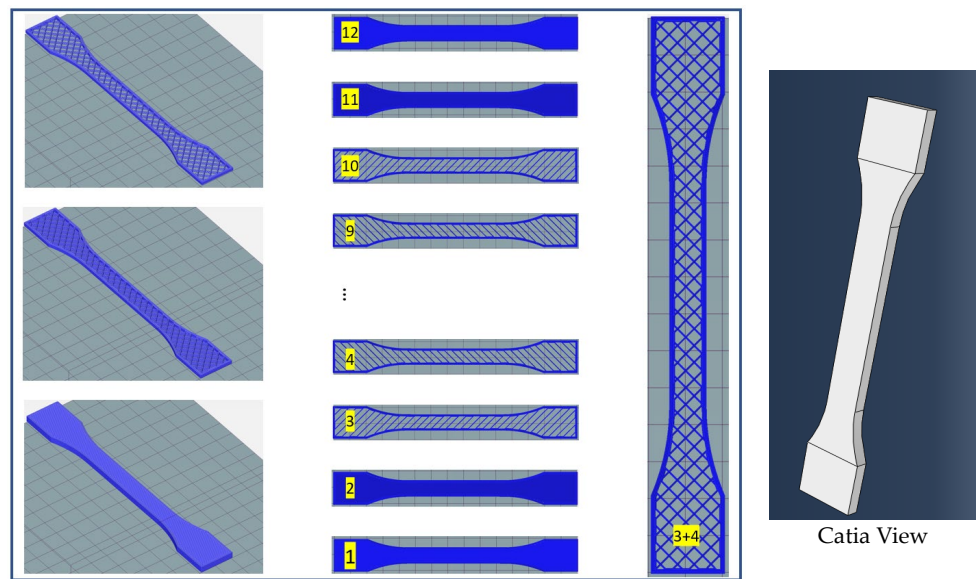
Table 2 summarizes the printing characteristics of all the samples. Two different CF/PETG composite configurations, Nida and rectilinear, were tested experimentally. The FDM process was used to create specimens with dimensions of 151.8 mm in length, 4 mm in thickness, and 21.8 mm in width. While fabricating the specimens, the infill densities were varied to better understand the mechanical properties. All specimens used to test the effect of filling density were made with the two filling patterns (NIDA and REC), with filling densities of 20%, 50%, 75%, and 100%, as shown in Figure 2.

Table 2. (A) The print properties of the CF/PETG and (B) the print statistics.

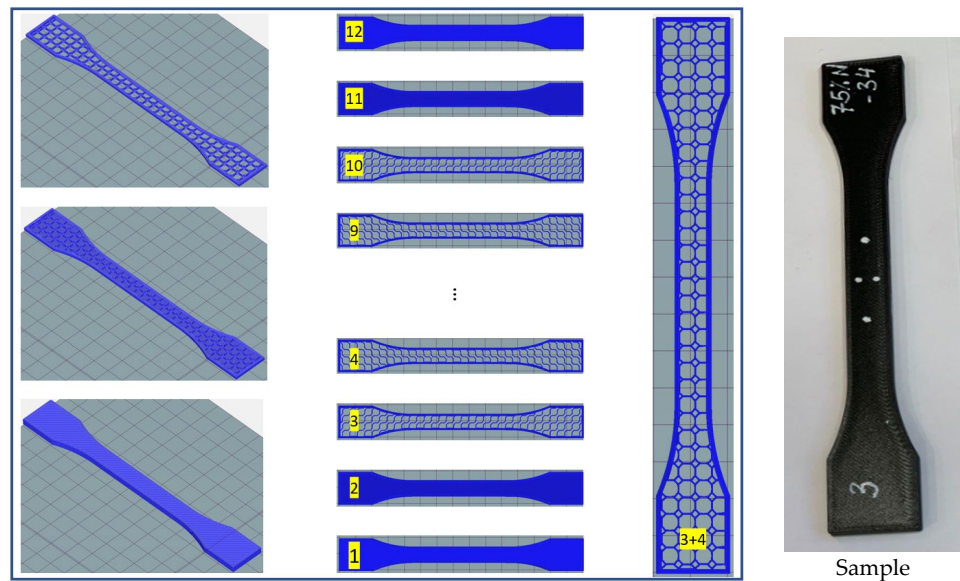
(A)	Print Properties of the CF/PETG	
Extrusion temperature	395	(°C)
Plate temperature	165	(°C)
Nozzle	0.5	(mm)
Print speed	40	(mm/s)
Layer thickness	0.3	(mm)

Table 2. Cont.

(B)		Number of Layers	Total Rows	Filament Required (mm)	Print Time
Rectilinear	20%	12	11,140	871	0 h, 40 mn, 36 s
	50%	12	12,369	1064	0 h, 47 mn, 01 s
	75%	12	12,369	1272	0 h, 47 mn, 01 s
Honeycomb	20%	12	12,832	882	0 h, 41 mn, 04 s
	50%	12	35,752	1226	0 h, 54 mn, 06 s
	75%	12	35,752	1515	0 h, 54 mn, 06 s
	100%	12	15,875	1438	1 h, 03 mn, 21 s



(a) Printing with a rectilinear pattern of 20%.



(b) Printing with a Nida pattern of 20%.

Figure 2. The 3D printing system and the differences between the two infill patterns.

As has already been said, the specifications of each print job should be considered when choosing a filler. Saving money and time without compromising the durability of a material is the fundamental justification for printing less than 100 percent of a filling piece. Table 2 shows the total number of printed pieces and a comparison of the various filling densities in terms of the amount of time and material required for printing.

4. Tensile Tests

The tensile test stands out as the most fundamental among the different mechanical tests used to fully comprehend and characterize the behaviors of materials. With its vital insights into the mechanical properties of materials, this specific testing technique is a cornerstone in materials research and engineering. The tensile test can identify critical properties that define a material's mechanical behavior. These essential characteristics include the ultimate tensile strength (UTS), indicating the most significant stress and strain a material can sustain without rupturing. The tensile test also offers information on the material's tensile strength, which measures the most incredible pressure it can withstand. Other crucial mechanical characteristics derived from the tensile test include yield strength, the stress point at which the material starts to demonstrate plastic deformation, and elongation at break, which reveals the material's ductility and capacity to deform before fracturing. The test also provides information on the material's stiffness (its Young's modulus) and lateral contraction in response to axial stretching (its Poisson's ratio). The tensile test procedure in this study entailed applying a continuous strain at a set rate to a specimen with a dumbbell shape.

The quasi-static tests were performed on an Instron electromechanical testing machine (a type 5585H universal traction machine) equipped with a 10 kN force cell and an INSTRON AVE 2663-821 model video extensometer (Figure 3 (1)). A computer ran the test through the Bluehill modular software (<https://www.instron.com/en/products/materials-testing-software/bluehill-universal> accessed on 1 March 2024) (Figure 3). The tensile force was applied to a sample until it broke at a constant speed according to the charging process. The two ends of the sample were clamped, and sliding was prevented by using sandpaper stuck onto the clamps. The samples were loaded with a displacement speed of 2 mm/min. All tests were performed at an ambient temperature and repeated three to five times on different specimens of the same shape to ensure repeatable results. Conducting tests to characterize the mechanical properties and measure the magnitude (stress and deformation) did not cause any particular problems.

Results

It was essential to establish and guarantee the reproducibility of the test procedure before carrying out the quasi-static tensile tests on the INSTRON machine. To this end, a thorough evaluation of each specimen was carried out to confirm the accuracy and reliability of the test results. Samples were subjected to the tensile test technique at least three times for this evaluation, with different filling patterns and densities at each iteration. In this way, we hoped to ensure that the results were not influenced by chance or external variables, guaranteeing subsequent test results' accuracy and consistency. This comprehensive testing technique underlined our commitment to the accuracy and reliability of our research results.

Figure 4 presents the force vs. displacement curves obtained for the different filling densities of the CF/PETG with honeycomb (NIDA) and rectilinear (REC) filling patterns. Figure 4 depicts a representative repeatable force vs. displacement variation for the different CF/PETG filling densities.

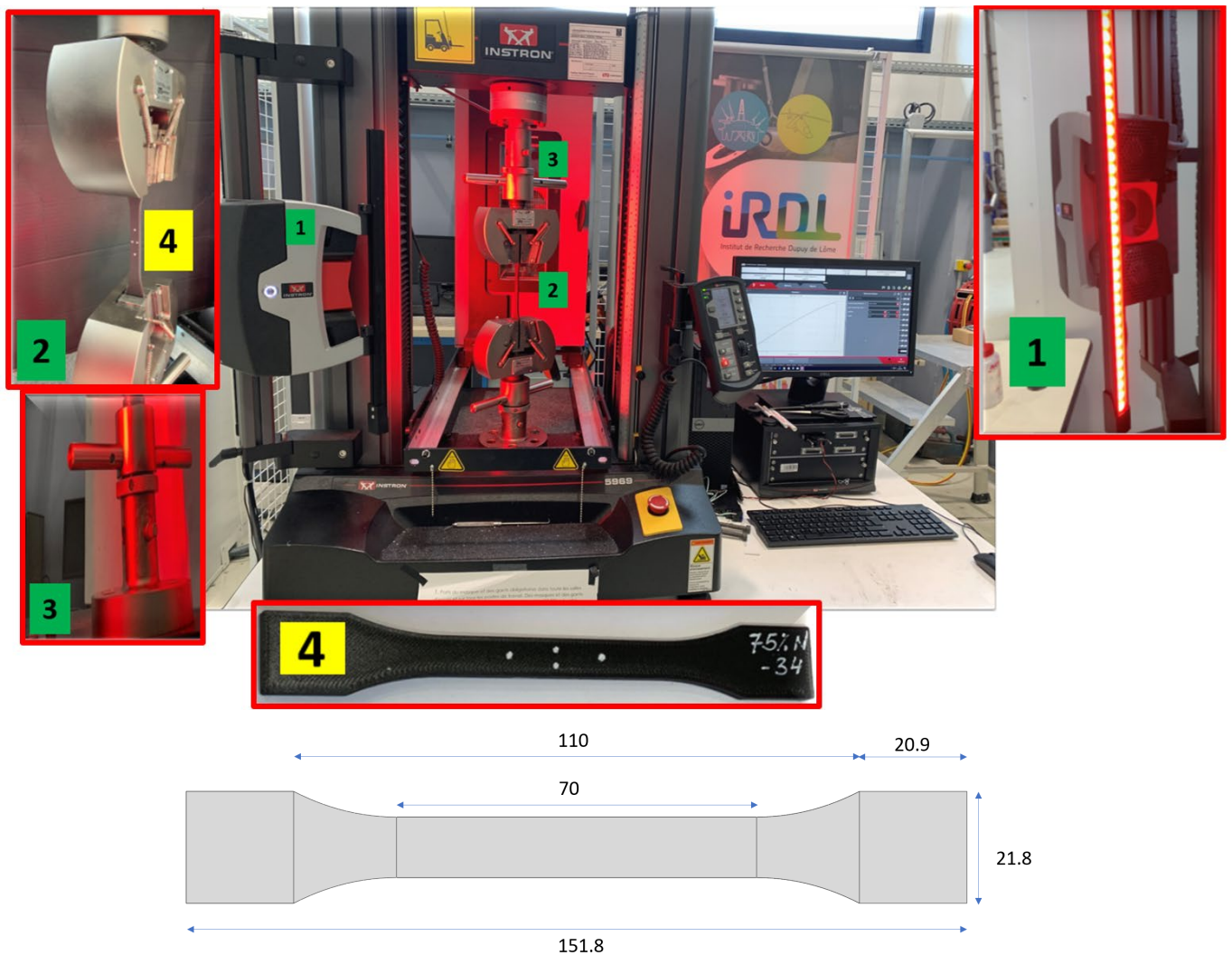
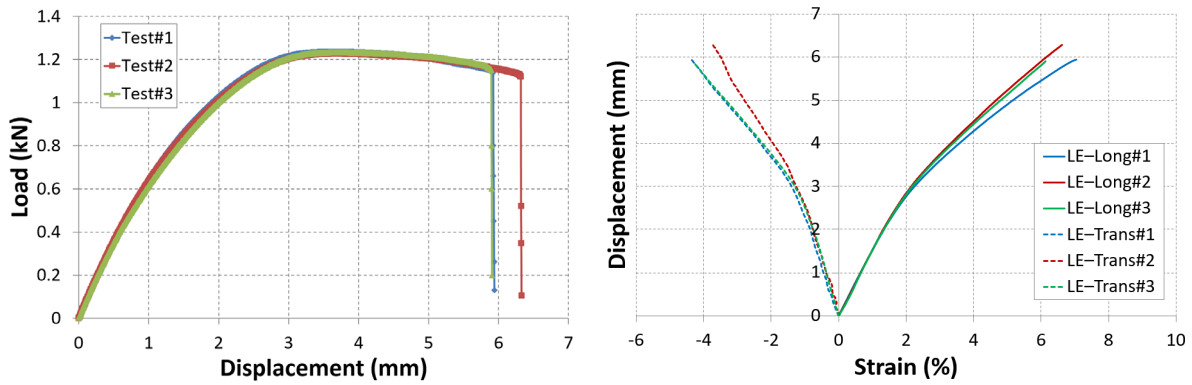


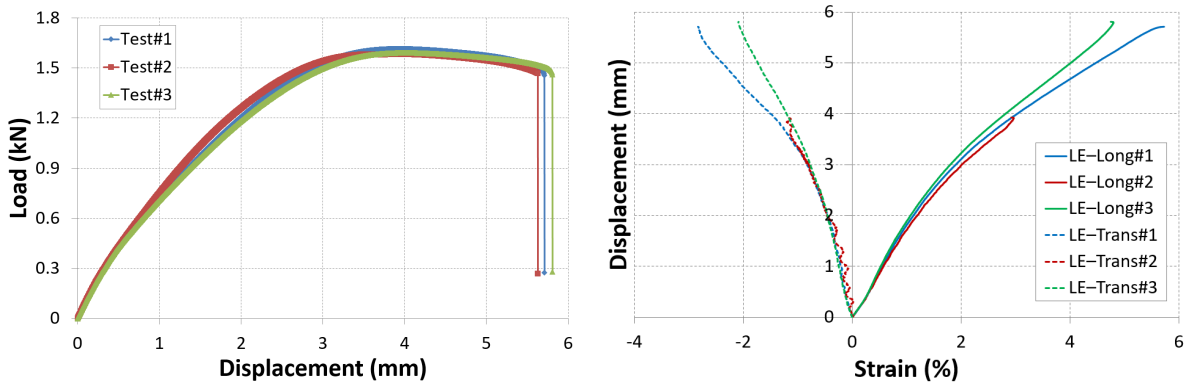
Figure 3. Components of the traction machine.

As seen in Figure 5, no particular infill pattern was formed by the infill densities in the 100% specimen created by the slicing program MakerBot Makerware. The data collected at the 100% infill density were used as the control variable for the comparative study.

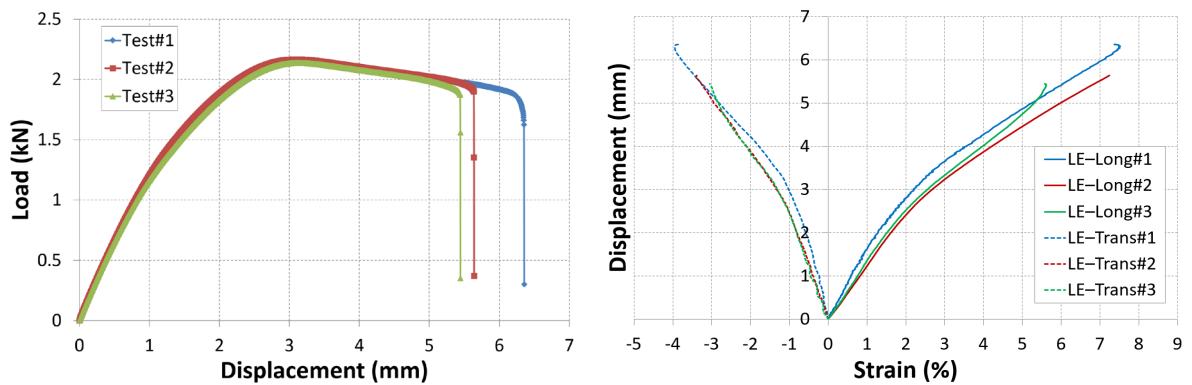
Figure 5a,b depicts the behavior variations for the two filling patterns with different infill densities. It shows that specimens manufactured with 100% infill densities had the highest resistance in the tensile tests compared to the honeycomb and rectilinear filling specimens. The mechanical behavior of samples with densities of 20–50% infill decreased significantly. This relationship was nearly linear, and the peak stress was proportional to the infill densities in the honeycomb and rectilinear filling patterns. This finding indicated that the infill density significantly impacted the mechanical properties of the CF/PETG sample.



(a) The 50% RECT pattern.



(b) The 50% NIDA pattern.



(c) The 100% pattern.

Figure 4. Examples of test reproducibility for the NIDA and RECT patterns.

The Young’s moduli and tensile strengths rose with the increasing infill densities, according to the experimental results of the printed composite structures with various infill densities. These could be compared to the enhanced deformation resistance capabilities of the composite structures.

The ultimate tensile strength of the CF/PETG with the two infill patterns (Nida and REC) and the different density percentages (20%, 50%, 75%, and 100%) were tested using an Instron tensile machine with an additionally connected extensometer. The values with error bars are shown in Figure 5c and Tables 3 and 4.

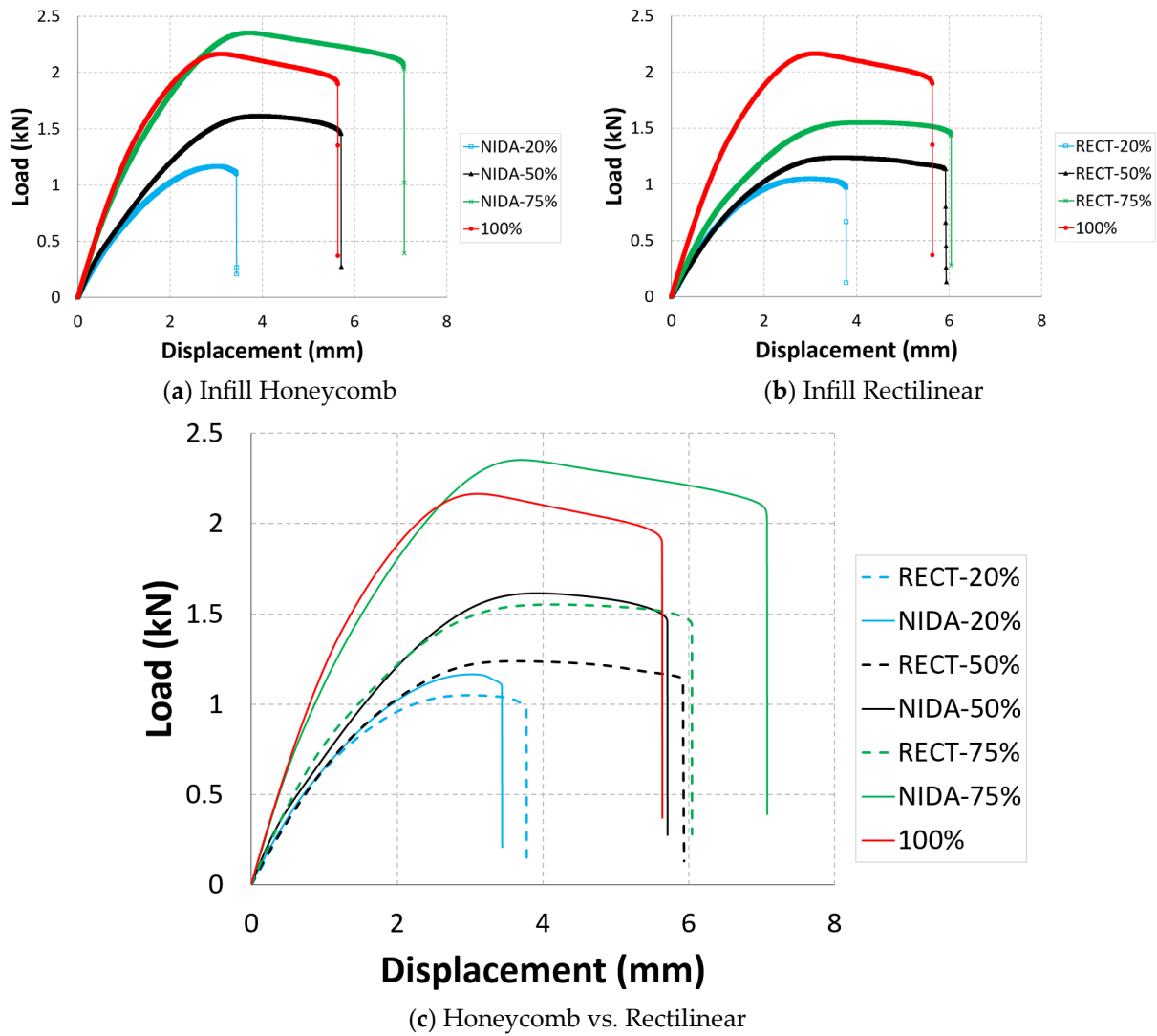


Figure 5. Force vs. displacement curve for the honeycomb and rectilinear infill patterns.

Table 3. Summary of the behavior results of the 3D-printed honeycomb samples.

		E (GPa)	Poisson's Ratio	U Max (mm)	F Max (kN)	LE_Longi Max (%)	Stiffness (N/mm)	UTS (Mpa)
20%	Average	2.276	0.46	3.36	1.16	3.02	830.267	28.957
	St-Dev	0.151	0.05	0.23	0.02	0.60	53.545	0.611
50%	Average	2.861	0.40	5.72	1.60	5.38	939.054	39.904
	St-Dev	0.071	0.04	0.09	0.02	0.51	13.679	0.409
75%	Average	3.730	0.38	6.24	2.34	6.00	1309.669	47.626
	St-Dev	0.174	0.04	0.79	0.02	1.23	29.067	0.594
100%	Average	3.545	0.49	5.81	2.14	6.80	1361.629	53.492
	St-Dev	0.601	0.03	0.48	0.02	1.03	6.203	0.611

Table 4. Summary of the behavior results of the 3D-printed rectilinear samples.

		E (Gpa)	Poisson's Ratio	U Max (mm)	F Max (kN)	LE_Longi Max (%)	Stiffness (N/mm)	UTS (MPa)
20%	Average	2.138	0.49	3.67	1.05	3.51	738.374	26.199
	St-Dev	0.046	0.01	0.23	0.00	0.73	15.345	0.040
50%	Average	2.105	0.59	6.35	1.23	7.73	737.611	30.843
	St-Dev	0.032	0.03	0.46	0.00	1.74	1.06115	0.118
75%	Average	2.607	0.47	5.90	1.54	5.56	900.791	38.564
	St-Dev	0.080	0.02	0.45	0.01	1.04	11.577	0.319
100%	Average	3.545	0.49	5.81	2.14	6.80	1361.629	53.492
	St-Dev	0.601	0.03	0.48	0.02	1.03	6.203	0.611

The ultimate tensile strengths of the CF/PETG samples at the different infill densities for the honeycomb filling method were 13.28, 18.31, and 21.85 MPa. The tensile strength increased progressively as the infill density continued to increase. The Young's modulus increased as the infill density increased, (2276, 2861, and 3730 MPa for 20%, 50%, and 75%, respectively). At a 100% infill density, the CF/PETG had the maximum Young's modulus of 4148.59 MPa.

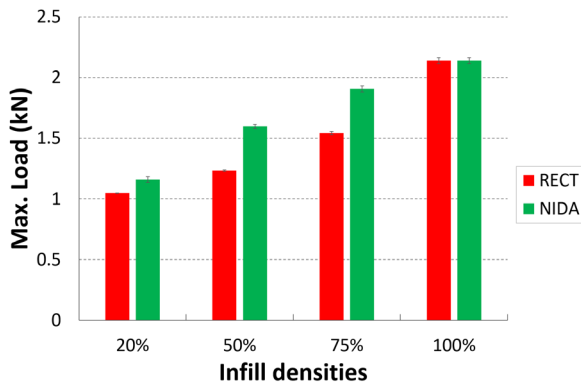
The ultimate tensile strength of the CF/PETG at 50% and 75% infill densities for the rectilinear filling pattern were 30.84 and 38.56 MPa. At a 100% infill density, the CF/PETG had the maximum tensile strength of 53.49 MPa. At a 100% infill density, the annealed CF/PETG had the maximum Young's modulus of 4148.59 MPa. The Young's modulus increased as the infilling density increased, with 2690.31 and 3350.37 for 50% and 75%, respectively.

Improved deformation resistance capabilities may have caused the enhanced Young's moduli and tensile strengths observed with the increased infill densities. Notably, the higher infill densities reduced the gaps in the composite structures, increasing the cross-sectional areas that could effectively support the tensile loads [32].

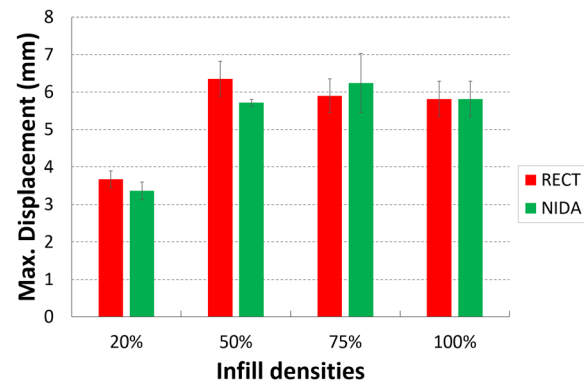
Furthermore, these variabilities were related to the printed parts' orientations, preferred reinforcements, post-processing, and infill densities. The tensile modulus of each printed specimen was increased by transversal printing. The infill density significantly impacted the strength of the printed specimen. The space between each layer was too close at a 100% infill density, which may have increased the high bonding strength between each printed layer [33], as shown in Figure 6.

Figure 5a,b demonstrates that the elongations at the breaks of the composites increased with the decreasing filling densities for the two types of filling patterns, increasing the total relative energy absorption. The composite specimens with higher infill densities had higher stiffness and tensile strengths. Elongations, on the other hand, decreased as the infill densities increased.

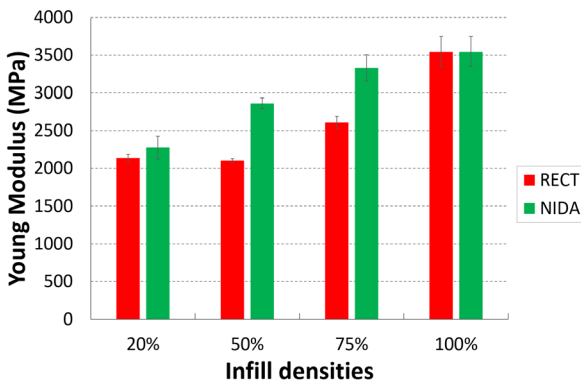
A higher defect density with more connecting nodes may have caused a decrease in the elongation associated with the high infill densities in the composite constructions. All printed specimens contained manufacturing flaws in the internal nodes of the cells because of the numerous crossovers of fused filaments created by the printing process [34,35], as seen in Figure 5a,b.



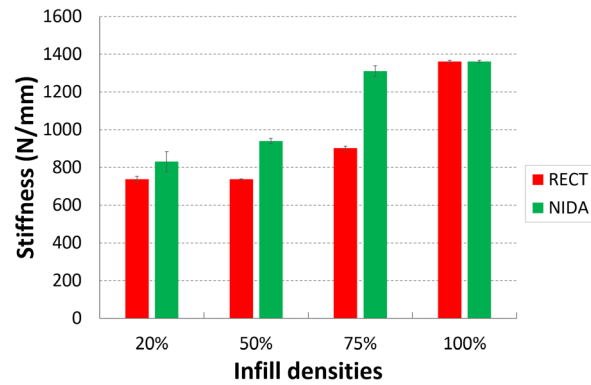
(a) Load variation as a function of fill rate



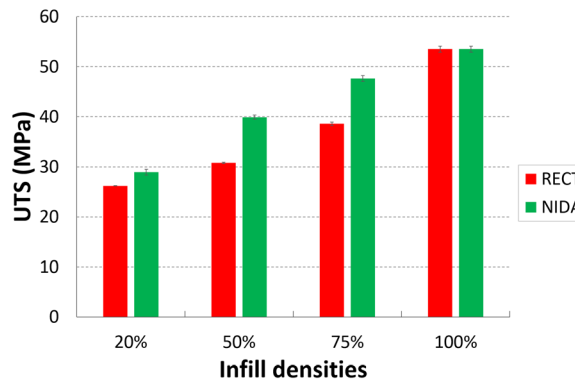
(b) Displacement variation as a function of fill rate



(c) Young modulus variation as a function of fill rate



(d) Stiffness variation as a function of fill rate



(e) Ultimate tensile strength variation (UTS) as a function of fill rate.

Figure 6. Comparative study between the honeycomb and rectilinear infill patterns.

The increased imperfection density and decreased elongation may have affected the higher infill density specimens [36]. Another reason for the increased elongation in the specimens with lower infill densities was the extended structure in each unit [37], as seen in Figure 5.

The maximal forces of the composite samples with the two distinct infill patterns resulted in similar stress distributions on the structures that were dependent on the infill densities during the static tensile deformation.

As a result, the infill density had little effect on the failure mode, except for the low-density percentage of 20%, which degraded in a short period of time.

As with the 50%, 75%, and 100% densities, a prominent unit structure would typically permit more rotation space and flexibility along the axial extension direction, resulting in a higher elongation for a composite construction.

As shown in Figure 5c, at varying infill densities, the composites with honeycomb infill structures were stiffer and less ductile than those filled with rectilinear units.

Figure 6 shows that the composite constructions with honeycomb infill patterns had better Young's moduli, and this was linked to the beam theory.

5. Conclusions

A filling must be selected for the unique requirements of a print job, as stated in the introduction. Therefore, filling density is decided based on the application needed.

One of the benefits of 3D printing FDM technology is that product lines can be produced with varying infill densities. This benefit reduces the time and material used and the cost of the finished product. After analyzing the tensile testing results, it was possible to conclude that:

- The infill types and densities affect the ultimate tensile strengths and yield strengths.
- The ultimate tensile strengths and yield strengths of all types of infill patterns increase as the density increases from 20% to 75%. Maximum strength is achieved with a 75% infill.
- The results showed that the honeycomb infill pattern had the highest ultimate tensile strength and yield strength when compared to the rectilinear infill.
- Compared to the 100% infill, the honeycomb and rectilinear infill patterns of 75% resulted in slightly lower ultimate tensile strengths.

The effects of infill patterns and densities on material properties were investigated in this paper only for tensile testing in one direction and for one printing orientation. Other factors to consider in future examinations include different printing orientations and testing in three directions. In addition, the effects of infill patterns and densities on other material properties (bending, pressure, hardness, and so on) should be investigated.

Furthermore, it will be necessary for companies to calculate the amount of filament to use and the printing time required due to filling in to determine if 3D printing remains profitable.

Author Contributions: The authors confirm that their contributions to the article were as follows: study design: M.D. and M.T.; experimental study: M.D.; data collection: M.D., M.T. and M.B.; analysis and interpretation of results: M.D., M.T., A.B. and M.B.; writing of the manuscript: M.D. and M.T. All authors have read and agreed to the published version of the manuscript.

Funding: This research received no external funding.

Data Availability Statement: Data are contained within the article.

Conflicts of Interest: The authors declare no conflict of interest. This manuscript is original, has not been published before, and is not currently being considered for publication elsewhere.

References

1. Grünewald, J.; Parlevliet, P.; Altstädt, V. Manufacturing of thermoplastic composite sandwich structures: A review of literature. *J. Thermoplast. Compos. Mater.* **2017**, *30*, 437–464. [[CrossRef](#)]
2. El Moumen, A.; Tarfaoui, M.; Lafdi, K. Additive manufacturing of polymer composites: Processing and modeling approaches. *Compos. Part B Eng.* **2019**, *171*, 166–182. [[CrossRef](#)]
3. Rouway, M.; Nachtane, M.; Tarfaoui, M.; Chakhchaoui, N.; Omari, L.E.H.; Fraija, F.; Cherkaoui, O. 3D printing: Rapid manufacturing of a new small-scale tidal turbine blade. *Int. J. Adv. Manuf. Technol.* **2021**, *115*, 61–76. [[CrossRef](#)]
4. Daly, M.; Tarfaoui, M.; Chihi, M.; Bouraoui, C. FDM technology and the effect of printing parameters on the tensile strength of ABS parts. *Int. J. Adv. Manuf. Technol.* **2023**, *126*, 5307–5323. [[CrossRef](#)]
5. Nachtane, M.; Tarfaoui, M.; Ledoux, Y.; Khammassi, S.; Leneveu, E.; Pelleter, J. Experimental investigation on the dynamic behavior of 3D printed CF-PEKK composite under cyclic uniaxial compression. *Compos. Struct.* **2020**, *247*, 112474. [[CrossRef](#)]
6. Tarfaoui, M.; Nachtane, M.; Goda, I.; Qureshi, Y.; Benyahia, H. 3D printing to support the shortage in personal protective equipment caused by COVID-19 pandemic. *Materials* **2020**, *13*, 3339. [[CrossRef](#)] [[PubMed](#)]
7. Javaid, M.; Haleem, A. Additive manufacturing applications in medical cases: A literature based review. *Alex. J. Med.* **2018**, *54*, 411–422. [[CrossRef](#)]

8. Goda, I.; Nachtane, M.; Qureshi, Y.; Benyahia, H.; Tarfaoui, M. COVID-19: Current challenges regarding medical healthcare supplies and their implications on the global additive manufacturing industry. *Proc. Inst. Mech. Eng. Part H J. Eng. Med.* **2020**, *236*, 613–627. [[CrossRef](#)] [[PubMed](#)]
9. Goda, I.; Reis, F.D.; Ganghoffer, J.-F. Limit analysis of lattices based on the asymptotic homogenization method and prediction of size effects in bone plastic collapse. In *Generalized Continua as Models for Classical and Advanced Materials*; Springer: Berlin/Heidelberg, Germany, 2016; pp. 179–211.
10. Goda, I.; Rahouadj, R.; Ganghoffer, J.-F. Size dependent static and dynamic behavior of trabecular bone based on micromechanical models of the trabecular architecture. *Int. J. Eng. Sci.* **2013**, *72*, 53–77. [[CrossRef](#)]
11. Picard, M.; Mohanty, A.K.; Misra, M. Recent advances in additive manufacturing of engineering thermoplastics: Challenges and opportunities. *RSC Adv.* **2020**, *10*, 36058–36089. [[CrossRef](#)]
12. Shanmugam, V.; Das, O.; Neisiany, R.E.; Babu, K.; Singh, S.; Hedenqvist, M.S.; Berto, F.; Ramakrishna, S. Polymer Recycling in Additive Manufacturing: An Opportunity for the Circular Economy. *Mater. Circ. Econ.* **2020**, *2*, 11. [[CrossRef](#)]
13. Yaragatti, N.; Patnaik, A. A review on additive manufacturing of polymers composites. *Mater. Today Proc.* **2020**, *44*, 4150–4157. [[CrossRef](#)]
14. Goda, I.; Ganghoffer, J.-F. 3D plastic collapse and brittle fracture surface models of trabecular bone from asymptotic homogenization method. *Int. J. Eng. Sci.* **2015**, *87*, 58–82. [[CrossRef](#)]
15. Rybachuk, M.; Mauger, C.A.; Fiedler, T.; Öchsner, A. Anisotropic mechanical properties of fused deposition modeled parts fabricated by using acrylonitrile butadiene styrene polymer. *J. Polym. Eng.* **2017**, *37*, 699–706. [[CrossRef](#)]
16. Mwema, F.M.; Akinlabi, E.T.; Mwema, F.M.; Akinlabi, E.T. Basics of fused deposition modelling (FDM). In *Fused Deposition Modeling: Strategies for Quality Enhancement*; Springer: Berlin/Heidelberg, Germany, 2020; pp. 1–15.
17. Shanmugam, V.; Das, O.; Babu, K.; Marimuthu, U.; Veerasimman, A.; Johnson, D.J.; Neisiany, R.E.; Hedenqvist, M.S.; Ramakrishna, S.; Berto, F. Fatigue behaviour of FDM-3D printed polymers, polymeric composites and architected cellular materials. *Int. J. Fatigue* **2021**, *143*, 106007. [[CrossRef](#)]
18. Tao, Y.; Wang, H.; Li, Z.; Li, P.; Shi, S.Q. Development and Application of Wood Flour-Filled Polylactic Acid Composite Filament for 3D Printing. *Materials* **2017**, *10*, 339. [[CrossRef](#)] [[PubMed](#)]
19. Abbas, T.; Othman, F.M.; Ali, H.B. Effect of infill Parameter on compression property in FDM Process. *Dimensions* **2017**, *12*, 24–25.
20. Alvarez, C.K.L.; Lagos, C.R.F.; Aizpun, M. Investigating the influence of infill percentage on the mechanical properties of fused deposition modelled ABS parts. *Ing. Investig.* **2016**, *36*, 110–116. [[CrossRef](#)]
21. Rismalia, M.; Hidajat, S.C.; Permana, I.G.R.; Hadisujoto, B.; Muslimin, M.; Triawan, F. Infill pattern and density effects on the tensile properties of 3D printed PLA material. *J. Phys. Conf. Ser.* **2019**, *1402*, 044041. [[CrossRef](#)]
22. Yang, L.; Harrysson, O.; West, H.; Cormier, D. Mechanical properties of 3D re-entrant honeycomb auxetic structures realized via additive manufacturing. *Int. J. Solids Struct.* **2015**, *69–70*, 475–490. [[CrossRef](#)]
23. Fadida, R.; Rittel, D.; Shirizly, A. Dynamic Mechanical Behavior of Additively Manufactured Ti6Al4V With Controlled Voids. *J. Appl. Mech.* **2015**, *82*, 041004. [[CrossRef](#)]
24. Tsouknidas, A.; Pantazopoulos, M.; Katsoulis, I.; Fasnakis, D.; Maropoulos, S.; Michailidis, N. Impact absorption capacity of 3D-printed components fabricated by fused deposition modelling. *Mater. Des.* **2016**, *102*, 41–44. [[CrossRef](#)]
25. Fernandez-Vicente, M.; Calle, W.; Ferrandiz, S.; Conejero, A. Effect of Infill Parameters on Tensile Mechanical Behavior in Desktop 3D Printing. *3D Print. Addit. Manuf.* **2016**, *3*, 183–192. [[CrossRef](#)]
26. Wyatt, H.; Safar, A.; Clarke, A.; Evans, S.L.; Mihai, L.A. Nonlinear scaling effects in the stiffness of soft cellular structures. *R. Soc. Open Sci.* **2019**, *6*, 181361. [[CrossRef](#)] [[PubMed](#)]
27. Zhang, P.; Arceneaux, D.J.; Khattab, A. Mechanical properties of 3D printed polycaprolactone honeycomb structure. *J. Appl. Polym. Sci.* **2017**, *135*. [[CrossRef](#)]
28. Antolak-Dudka, A.; Piatek, P.; Durejko, T.; Baranowski, P.; Małachowski, J.; Sarzyński, M.; Czujko, T. Static and Dynamic Loading Behavior of Ti6Al4V Honeycomb Structures Manufactured by Laser Engineered Net Shaping (LENSTM) Technology. *Materials* **2019**, *12*, 1225. [[CrossRef](#)]
29. Bates, S.R.; Farrow, I.R.; Trask, R.S. Compressive behaviour of 3D printed thermoplastic polyurethane honeycombs with graded densities. *Mater. Des.* **2018**, *162*, 130–142. [[CrossRef](#)]
30. Yu, S.; Sun, J.; Bai, J. Investigation of functionally graded TPMS structures fabricated by additive manufacturing. *Mater. Des.* **2019**, *182*, 108021. [[CrossRef](#)]
31. Le Plastique PETG en Impression 3D. Available online: <https://www.3dnatives.com/plastique-petg-18122019/#!> (accessed on 1 August 2023).
32. Dawoud, M.; Taha, I.; Ebeid, S.J. Mechanical behaviour of ABS: An experimental study using FDM and injection moulding techniques. *J. Manuf. Process.* **2016**, *21*, 39–45. [[CrossRef](#)]
33. Kumar, K.S.; Soundararajan, R.; Shanthosh, G.; Saravanakumar, P.; Ratteesh, M. Augmenting effect of infill density and annealing on mechanical properties of PETG and CFPETG composites fabricated by FDM. *Mater. Today Proc.* **2020**, *45*, 2186–2191. [[CrossRef](#)]
34. Zhou, X.; Zhang, J.; Yang, S.; Berto, F. Compression-induced crack initiation and growth in flawed rocks: A review. *Fatigue Fract. Eng. Mater. Struct.* **2021**, *44*, 1681–1707. [[CrossRef](#)]
35. du Plessis, A.; Yadroitsev, I.; Yadroitsava, I.; Le Roux, S.G. X-Ray Microcomputed Tomography in Additive Manufacturing: A Review of the Current Technology and Applications. *3D Print. Addit. Manuf.* **2018**, *5*, 227–247. [[CrossRef](#)]

36. Wang, K.; Xie, X.; Wang, J.; Zhao, A.; Peng, Y.; Rao, Y. Effects of infill characteristics and strain rate on the deformation and failure properties of additively manufactured polyamide-based composite structures. *Results Phys.* **2020**, *18*, 103346. [[CrossRef](#)]
37. Lubombo, C.; Huneault, M.A. Effect of infill patterns on the mechanical performance of lightweight 3D-printed cellular PLA parts. *Mater. Today Commun.* **2018**, *17*, 214–228. [[CrossRef](#)]

Disclaimer/Publisher’s Note: The statements, opinions and data contained in all publications are solely those of the individual author(s) and contributor(s) and not of MDPI and/or the editor(s). MDPI and/or the editor(s) disclaim responsibility for any injury to people or property resulting from any ideas, methods, instructions or products referred to in the content.